The Astrophysical Journal, 747:68 (11pp), 2012 March 1 doi:10.1088/0004-637X/747/1/68

AGES AND METALLICITIES OF CLUSTER GALAXIES IN A779 USING MODIFIED STRÖMGREN PHOTOMETRY

Yuvraj Harsha Sreedhar[1], Andrew P. Odell[2], Karl D. Rakos[1], Gerhard Hensler[1], and Werner W. Zeilinger[1]
[1] University of Vienna, Institute of Astronomy, Türkenschanzstraße 17, A-1180 Vienna, Austria
[2] Department of Physics and Astronomy, Northern Arizona University, Flagstaff, AZ, USA
Received 2010 November 23; accepted 2011 December 6; published 2012 February 15

ABSTRACT

In the quest for the formation and evolution of galaxy clusters, Rakos and co-workers introduced a spectrophotometric method using modified Strömgren photometry, but with the considerable debate toward the project's abilities, we re-introduce the system by testing for the repeatability of the modified Strömgren colors and compare them with the Strömgren colors, and check for the reproducibility of the ages and metallicities (using the Principle Component Analysis (PCA) technique and the GALEV models) for the six common galaxies in all three A779 data sets. As a result, a fair agreement between two filter systems was found to produce similar colors (with a precision of 0.09 mag in $(uz - vz)$, 0.02 mag in $(bz - yz)$, and 0.03 mag in $(vz - vz)$) and the generated ages and metallicities are also similar (with an uncertainty of 0.36 Gyr and 0.04 dex from PCA and 0.44 Gyr and 0.2 dex using the GALEV models). We infer that the technique is able to relieve the age–metallicity degeneracy by separating the age effects from the metallicity effects, but it is still unable to completely eliminate it. We further extend this paper to re-study the evolution of galaxies in the low mass, dynamically poor A779 cluster (as it was not elaborately analyzed by Rakos and co-workers in their previous work) by correlating the luminosity (mass), density, and radial distance with the estimated age, metallicity, and the star formation history. Our results distinctly show the bimodality of the young, low-mass, metal-poor population with a mean age of 6.7 Gyr ($\pm$ 0.5 Gyr) and the old, high-mass, metal-rich galaxies with a mean age of 9 Gyr ($\pm$ 0.5 Gyr). The method also observes the color evolution of the blue cluster galaxies to red (Butcher–Oemler phenomenon), and the downsizing phenomenon. Our analysis shows that modified Strömgren photometry is very well suited for studying low- and intermediate-z clusters, as it is capable of observing deeper with better spatial resolution at spectroscopic redshift limits, and the narrowband filters estimate the age and metallicity with fewer uncertainties compared to other methods that study stellar population scenarios.

Key words: galaxies: clusters: individual (A779) – galaxies: elliptical and lenticular, cD – galaxies: evolution – galaxies: formation – galaxies: photometry – galaxies: star formation

Online-only material: color figures

1. INTRODUCTION

The initial use of the Strömgren filter system was to study stars by Strömgren (1966), where one could exploit the filter's sensitive nature to detect individual stellar parameters. However, Rakos et al. (1988) used these filters, with slight modifications, to analyze galaxy evolution in clusters at their rest frame. Using this unique feature of rest-frame Strömgren photometry, we compare and analyze the results of A779 cluster galaxies. The cluster A779 has been studied by many authors (Kellogg et al. 1973; Huchra et al. 1992; White et al. 1997; Jones & Forman 1984; David et al. 1993; Zabludoff et al. 1993; Hwang & Lee 2008) in different wavelengths and using different techniques which presented intriguing results on the cluster's formation and evolution. Previously, Rakos et al. (2008) had cumulatively studied eight clusters, including A779. Since its evolutionary properties were significantly overshadowed by the other rich clusters in their study (Fornax, Coma, A1185, A2218, the X-ray bright clusters like A539, A119 and the X-ray, radio bright cluster A400), we investigate the formation and evolution of galaxies in A779 separately.

Also, since the rest-frame narrowband galaxy analysis technique along with its abilities are often debated in the scientific community, a thorough testing of this method becomes mandatory. In order to do so and to show its robustness, we have carried out a repeatability test of the observed A779 galaxy colors obtained from two different observations and compared it with the previously published results of Rakos et al. (2008). The three observations compared here are conducted using two filter systems: Strömgren and modified Strömgren photometry (defined in Section 2).

Primary parameters like the ages and metallicities of galaxies reflect the underlying star formation history and the chemical evolution of galaxies, respectively, but their measurements and reliability are often model-dependent and inaccurate. In addition, the age–metallicity degeneracy (Worthey 1994, 1999) further affects their measurements, caused by the contribution of the main-sequence turnoff stars, which are sensitive to age, and the red giant branch (RGB) stars, which are sensitive to metallicity. In order to relieve this degeneracy, Rakos et al. (1996) took advantage of the narrowband filters that focus only on certain regions of the galaxy spectrum which are sensitive to either age or metallicity. To further isolate these two parameters, Rakos & Schombert (2005a, henceforth R05a) implemented the Principle Component Analysis (PCA; Steindling et al. 2001) technique on Schulz et al.'s (2002, henceforth S02) evolutionary models. As an evaluation, we compare the ages and metallicities (obtained from the observed A779 galaxy colors) determined from the PCA method with the advanced GALEV (Kotulla et al. 2009) evolutionary models.

Using our latest observations of 2009 December, we show the ability of our modified Strömgren photometry by observing a

Table 1
A779 X-Ray Properties from the Literature

X-Ray Property	Value
F_x[a]	$<8.5 \times 10^{-11}$ erg s^{-1} cm^{-2}
L_x[b]	0.09×10^{44} erg s^{-1}
L_x[c]	$2 \pm 0.19 \times 10^{43}$ erg s^{-1}
L_x[d]	$<0.09 \times 10^{43}$ erg s^{-1}
L_x[e]	$<1.20 \times 10^{43}$ erg s^{-1}
T_x[f]	1.5 keV
σ[g]	503^{100}_{-63} km s^{-1}
σ_p[h]	491^{40}_{-36} km s^{-1}

Notes.
[a] Kellogg et al. (1973) at 2–6 keV.
[b] Huchra et al. (1992) at 0.1–2.4 keV.
[c] White et al. (1997) bolometric X-rays luminosities.
[d] Jones & Forman (1984) using *Einstein* (soft, 0.5–3 keV).
[e] Compilation of *Einstein*, *EXOSAT*, and *Ginga* data from David et al. (1993).
[f] *Einstein* estimate of X-ray temperature from White et al. (1997).
[g] Radial velocity dispersion from Zabludoff et al. (1993).
[h] Radial velocity dispersion from Hwang & Lee (2008).

poor (Bautz-Morgan, BM class II), faint (with galaxy members of $M_{5500} \simeq -14.73$) A779 galaxy cluster and explore its evolutionary scenarios. It is interesting to study these small, poor clusters since they resemble the early clusters at high-z which indicate an accumulation of galaxies that form large clusters. By studying these low-mass, poor clusters using modified Strömgren photometry, we hope to discover and study some phenomena that may have been overlooked by other disparate studies. Therefore, we consider studies from other wavelengths predominantly to understand the cluster's formation and evolution.

Observations in the X-rays complement the cluster studies greatly by showing the underlying intracluster medium and hot gas, which forms the second massive cluster component after dark matter (∼80% cluster mass). Galaxies and the intergalactic medium (IGM) are known to be well connected by accretion (on to galaxies) and flows of matter and energy by the process of "Cosmic Feedback." Starburst galaxies expel matter by galactic-scale outflows or "superwinds" (originating from hot massive stars and core-collapse supernovae) to the IGM, polluting them with the newly synthesized metals from stars. A part of the lost material is recycled directly within the intergalactic environment, forming the tidal dwarf galaxies (TDGs) that are made out of tidally expelled colliding galaxies. These TDGs, which are commonly found near interacting systems (Weilbacher et al. 2000) like groups and clusters are formed by the unstable tidal H I content that collapses, transforming into H_2 gas and igniting the star formation (Duc et al. 2002). On the other hand, galaxies rotating through the hot IGM, depending upon their mass and morphology, experience ram-pressure stripping (Gunn & Gott 1972) which removes their ISM resulting in either low or no star formation.

A779 ($z = 0.023$) has been noted for its small size (75′ in radius, it resembles a galaxy group). With a BM class II and the Abell richness class of 0, it has a faint X-ray luminosity showing the presence of a very small amount of the X-ray-emitting gas. Table 1 presents A779's X-ray luminosity measurements by different authors from the literature up to the present. All these measurements present a low X-ray emission indicating smaller gas content with a gas temperature of 1.5 keV (White et al. 1997). Hwang & Lee's (2008) A779 study using Sloan Digital Sky Survey (SDSS) and 2dFGRS also detected very faint X-ray luminosity along with a mean galaxy radial velocity dispersion of 491^{+40}_{-36} km s^{-1}. Consistent with the studies of Oegerle & Hill (2001), Hwang & Lee (2008) also observed a cD galaxy, NGC 2832, at the center of A779 which is at rest in the cluster potential, and the presence of a large number of late-type galaxies compared to early types.

On the other hand, radio observations from the Westerbrock survey of cluster galaxies by Wilson & Vallée (1982) measure the peak map flux density for A779 to be 9 mJy. The two radio sources found at the cluster center, NGC 2832 and NGC 2831 (extended toward the NW–SE), form a double system in a halo. The direction of the radio source elongation seems similar to the optical halo. The core is dominated by the S0s and compact ellipticals, but no X-ray emission was detected by HEAO-2 and no radio emission was detected at a flux level of ∼5 mJy (Fanti 1984). A more recent 21 cm study by Solanes et al. (2001) inferred that the central ($r \leqslant 1$ Abell radius) and outer ($r \geqslant 1$ Abell radius) spiral populations of A779 have statistically significant reduced H I content. The peculiarity of this cluster comes from the H I-deficient components which show no statistically significant trend with cluster properties, such as the X-ray luminosity, temperature, velocity dispersion, and richness of the spiral fraction, which could be due to the higher rate of transformation of swept spirals into lenticulars in the richest X-ray clusters. The amount of gas depletion appears to be related to the morphology of the disks, but it is hardly a function of their optical size (Solanes et al. 2001).

With a view to test the method and to investigate the formation and evolution of galaxies in A779, this paper is arranged in the following sections. Section 2 describes the definition and the continuum colors of the modified Strömgren photometry. The results (Section 3) elaborate on the method for estimating galaxy ages and metallicities, and present the comparison of colors, model ages, and metallicities. The discussion section (Section 4) reports the evolution of A779 member galaxies using correlations of different galaxy parameters. Section 5 concludes the paper.

2. OBSERVATION

2.1. Modified Strömgren Photometry: The Definition

In the literature there are several definitions of the modified Strömgren filter system, most of which are not accurately defined. In principle, the modified Strömgren (uz, vz, bz, yz) filters are not much different from the normal Strömgren (u, v, b, y) filters, as the effective wavelength of the two filter systems is almost same. However, the modifications in the modified Strömgren filters come from the following aspects. (1) The uz filter is slightly (30 Å) shifted to the red to focus more on the red galaxies. (2) The calibration of these filters is performed using spectrophotometric standard stars that are shifted to the redshift of the target cluster (Rakos et al. 1988). This makes the zero point of the magnitudes differ along with the cluster's redshift. (3) The flux measurement for the galaxies and the standard stars is in wavelength units (per Å), as is usual for most galaxy studies instead of frequency (per Hz) units as in the stellar studies.

2.2. Narrowband Continuum Colors

The first set (2004 December) of A779 observations was obtained with the 2.3 m Bok telescope of the Steward Observatory which offers a 90″ prime image device with a prime-focus wide field imager and four 4k × 4k mosaic CCDs that observed a field of view of 1.°16 × 1.°16 and a plate scale of 0.″45 pixel^{-1} (Rakos et al. 2008). The observational attempts made in 2009 were to repeat the 2004 observations, but instead of four 4k × 4k mosaic CCDs only a single 4k × 4k CCD was used with field of view of 30′ × 30′ and a plate scale of 0.″45 pixel^{-1}. The observation at La Palma was performed using the 2.54 m INT prime-focus imager which has a field of view of 20′ × 40′; the wide field camera consists of 2k × 4k mosaic CCDs and a plate scale of 0.″33 pixel^{-1}.

The filter system used for the 2004 and 2009 observations at Steward Observatory is the same modified Strömgren system. Three exposures of 600 s were made in uz and vz and four exposures of 300 s were made in bz and yz for the 2004 observations. However, for the latest 2009 observations, three images of 600 s in uz and vz, three of 300 s in bz, and four of 300 s in yz were obtained. The calibration was obtained through a number of spectrophotometric standards measured on each night for the 2004 set of observations, but for 2009 observations the spectrophotometric standard measurements of four nights were averaged. The modified Strömgren filter system covers three regions in the near-UV and the blue portion of the electromagnetic spectrum. The bz ($\lambda_{\rm eff} = 4675$ Å) and yz ($\lambda_{\rm eff} = 5500$ Å) focus on the continuum part of the spectrum, both of which combine to form the temperature-color index ($bz - yz$). The vz ($\lambda_{\rm eff} = 4100$ Å) filter is strongly influenced by the metal absorption lines (i.e., Fe, CN) from the old stellar populations, whereas uz ($\lambda_{\rm eff} = 3500$ Å) is shortward of the Balmer jump. All the filters are sufficiently narrow (FWHM ∼ 200 Å) to sample the regions of spectrum that are unique to the determination of various physical parameters, such as star formation rate, age, and metallicity (Rakos et al. 2001). For the 2005 INT observation, the standard ($uvby$) filters were used and retained for analysis (by applying proper k-corrections to compare with the modified Strömgren filter system), wherein five exposures of 600s in each filter were made. Calibration was performed using the average of five nights of spectrophotometric standards.

The reduction procedure has been published in Rakos et al. (1996). The photometric system is based on the theoretical transmission curves of filters (which can be obtained upon request from the authors) and the spectra of the spectrophotometric standards are published by Massey & Gronwall (1990) and Hamuy et al. (1994). The convolution of the transmission curves and the spectra of the standard stars produce theoretical flux values for color indices of the standard stars corrected for all light losses in the equipment and the specific sensitivity of the CCD camera. Magnitudes are measured on the resultant co-added images using standard IRAF procedures and for brighter objects are based on metric apertures set at 32 kpc for cosmological parameters of $H_{\rm o} = 75$ km s^{-1} Mpc^{-1} and the benchmark cosmology ($\Omega_m = 0.3$, $\Omega_\Lambda = 0.7$). For the fainter objects, the apertures are adapted to deliver the best possible signal-to-noise ratio, but always using the same aperture for all four filters.

For the calculated colors, the galactic extinction toward A779 is found to be small: $E(B - V) = 0.017$ mag, which corresponds to $E(uz - vz) = 0.008$, $E(bz - yz) = 0.012$, and $E(vz - yz) = 0.019$. The effect of these corrections is negligible on the measured ages and metallicities (shown in Table 2). The limiting magnitude for all three observations is $13.05 \leqslant m_{5500} \leqslant 20.35$. The typical errors in colors for the three observations are in the range: $0.03 \leqslant (uz - vz) \leqslant 0.09$, $0.02 \leqslant (bz - yz) \leqslant 0.05$, and $0.03 \leqslant (vz - yz) \leqslant 0.07$. Using the photometric membership criteria, the foreground and background galaxies are removed (see Rakos et al. 1991 for a full description of the procedure) such that the member galaxies are found to be within 1000 km s^{-1} of the cluster mean redshift. This membership criterion resulted in cluster A779 having 45 galaxies in our 1° field of view. These member galaxies range from $13.3 \leqslant m_{5500} \leqslant 20.0$. Spectroscopic studies, on the other hand, of Hwang & Lee (2008) using the 3° field of view of SDSS and the 2° field of view of 2dFGRS find 145 cluster members for A779.

3. RESULTS

3.1. Method for Age and Metallicity Estimation

In the last two decades, the choice of techniques for estimating the ages and metallicities of galaxies has been the following. (1) Spectral energy distribution (SED) fitting of the age- and metallicity-sensitive spectral indices, through Lick indices (Trager et al. 2000; González 1993). (2) Spectrophotometric indices, for measuring the strength of specific features that are not sensitive to the flux calibration (Koleva et al. 2008). (3) Full spectrum fitting that uses all the redundant information contained in the signal. This last method is a combination of spectrophotometric indices and SED fitting (Koleva et al. 2008). Nevertheless, various age-sensitive indices are now found to contaminate the metallicity-sensitive indices and vice versa, which results in inaccurate and/or incorrect estimations of the two parameters (Worthey 1999). Ferreras et al. (1999) point out that the age-sensitive Hβ line is significantly affected by the nuclear emissions in the E/S0s for which corrections are uncertain (González 1993) and the [Mg/Fe] index changes drastically from faint to bright E/S0s, which challenges their use as a metallicity index.

A wealth of information on various age- or metallicity-sensitive spectral lines confuses their estimation. The strength of the Fe index shows hardly any dependence on the galaxy mass (Fischer et al. 1996). Sanchez-Blazquez et al. (2006) found that by using the Mg_2 index, no correlation in age and metallicity can be made; instead a clear trend is observed with the Ca and Fe indices. These challenges result in difficulties in painting a proper picture of galaxies since the evolutionary models do not use individual line strengths but the combined strength of several line indices which only point out the star's position on the Hertzsprung–Russell (H-R) diagram (Rakos et al. 2007). These ages, determined using the spectral indices, have recently been contradicted by many methods, for example, the Lick/IDS system which finds many cluster ellipticals of relatively younger ages of less than 6 Gyr (Sanchez-Blazquez et al. 2006); the photometric system using continuum colors detects only a few ellipticals less than 10 Gyr.

On the other hand, our method has the advantage of measuring the dominant component which produces the observed galaxy colors that are the continuum emission (Rakos et al. 2007) with high signal-to-noise ratio at relatively short exposures. The continuum colors are the primary source of information related to the characteristics of the underlying stellar populations. The age and metallicity determine the continuum emission through

Table 2
Comparison of Three Sets of Observations Showing the Narrowband Colors, M_{5500} Brightness, and the Age–Metallicity Estimations for All Six Objects Using Two Evolutionary Methods, PCA (using Schulz et al. 2002) and GALEV Models (Kotulla et al. 2009)

Obs.	Narrowband Colors				PCA		GALEV	
	$(uz-vz)$	$(bz-yz)$	$(vz-yz)$	$M(5500)$	[Fe/H] (dex)	Age (Gyr)	[Fe/H] (dex)	Age (Gyr)
Obj.1.								
INT	0.611	0.327	0.642	−20.164	−0.239	8.210	−0.3	8.680
90 P 2005	0.712	0.289	0.637	−20.266	−0.173	7.890	0.3	8.810
90 P 2009	0.599	0.324	0.636	−20.312	−0.316	8.690	0.3	8.400
Mean	0.641	0.313	0.638		−0.243	8.263	0.100	8.630
Obj.2.								
INT	0.742	0.366	0.690	−20.519	−0.017	9.350	0	9.050
90 P 2005	0.803	0.336	0.751	−20.613	0.028	9.63	0	9.380
90 P 2009	0.664	0.376	0.769	−20.687	0.048	8.810	0.3	8.570
Mean	0.736	0.359	0.737		0.020	9.263	0.100	9.000
Obj.3.								
INT	0.787	0.382	0.662	−19.395	0.055	8.700	0	9.180
90 P 2005	0.883	0.332	0.689	−19.637	0.079	8.700	0.3	9.810
90 P 2009	0.658	0.363	0.740	−19.680	0.041	7.980	0.3	8.550
Mean	0.776	0.359	0.697		0.058	8.460	0.200	9.180
More Data								
Obj. 4.								
INT	0.750	0.370	0.726	−19.276	0.032	9.290	0	9.200
90 P 2005	0.836	0.326	0.753	−19.379	0.082	8.960	0.3	9.390
90 P 2009	0.653	0.374	0.791	−19.449	0.076	8.470	0.3	8.560
Mean	0.746	0.357	0.757		0.063	8.907	0.200	9.050
Obj. 5.								
INT	0.742	0.379	0.735	−20.070	0.035	9.510	0	9.180
90 P 2005	0.901	0.348	0.724	−20.202	0.168	9.170	0	9.510
90 P 2009	0.679	0.385	0.767	−20.254	0.068	8.930	0.3	8.600
Mean	0.774	0.371	0.742		0.090	9.203	0.100	9.097
Obj. 6.								
INT	0.736	0.370	0.746	−19.853	0.072	8.630	0	9.170
90 P 2005	0.880	0.325	0.724	−19.939	0.072	9.120	0.3	9.470
90 P 2009	0.645	0.374	0.783	−20.007	0.030	8.950	0.3	8.550
Mean	0.754	0.356	0.751		0.058	8.900	0.200	9.063

the impact of the higher mass stars in the younger stellar populations (hot stars) and the changes in the color of the RGB by-line blanketing effects caused by the variation in the mean metallicity (Tinsley 1980), respectively.

R05a applied the PCA method[3] (Steindling et al. 2001) to S02's Single Stellar Population (SSP) models which are based on resolved isochrones of the Padova group. Briefly, PCA in any n-dimensional space calculates the axis with the most significant scatter as PC1, then the second most significant scatter in the remaining $n-1$ dimensional space, orthogonal to PC1 as PC2, and so on. The advantages of applying PCA are to reduce the dimensionality of the data and to provide the orthonormal coordinate system in which the data are most easily characterized. The original PC equations that are only color-dependent are

$$\mathrm{PC1} = 0.80(uz - vz) + 0.53(vz - bz) + 0.28(bz - yz) \quad (1)$$

$$\mathrm{PC2} = -0.56(uz - vz) + 0.49(vz - bz) + 0.67(bz - yz) \quad (2)$$

$$\mathrm{PC3} = 0.22(uz - vz) - 0.69(vz - bz) + 0.69(bz - yz). \quad (3)$$

[3] The program can be downloaded at http://student.fizika.org/~vkolbas/pca/index.html.

PCA is an empirical method based on the catalogs of galaxies and stellar population models (Kennicutt 1992a, 1992b; Kinney et al. 1996), which when applied to the S02 models offers the following advantages. (1) The PCA method helps in the selection of the cluster members using "the cluster box" (refer to Figure 2 in Steindling et al. 2001). (2) The classification of galaxies into different Hubble types is possible using this analysis technique. PCA allocates specific places for different galaxy morphological classes in "the cluster box" built by the three PC equations ((1)– (3)). (3) Importantly, PCA separates the age effects from the metallicity effects.

In order to apply PCA, the required linearity was observed for the SSPs with ages older than 3 Gyr for a full range of model metallicities. The primary reasons for the application of PCA are to separate the age and metallicity of a stellar population, select the most correlated variables, and to determine the linear combination of variables for extrapolation. Therefore, R05a adjusted these PC equations to include the model age and metallicity terms along with the observed colors as shown below

$$\mathrm{PC1} = 0.471[\mathrm{Fe/H}] + 0.175\tau + 0.480(uz - vz) + 0.506(bz - yz) + 0.511(vz - yz) \quad (4)$$

Table 3
Means and the Standard Deviations for the Observed Colors from the Three Sets of Observations and for the Measured Ages and Metallicities Using the PCA and GALEV Models

	Narrowband Colors			PCA		GALEV	
Object	$\sigma(uz-vz)$	$\sigma(bz-yz)$	$\sigma(vz-yz)$	σ[Fe/H]	σAge	σ[Fe/H]	σAge
Obj. 1	0.06	0.02	0.00	0.07	0.40	0.35	0.21
Obj. 2	0.07	0.02	0.04	0.03	0.42	0.17	0.41
Obj. 3	0.11	0.03	0.04	0.02	0.42	0.17	0.63
Obj. 4	0.09	0.03	0.03	0.03	0.41	0.17	0.43
Obj. 5	0.11	0.02	0.02	0.07	0.29	0.17	0.46
Obj. 6	0.12	0.03	0.03	0.02	0.25	0.17	0.47
Mean	0.09	0.02	0.03	0.04	0.36	0.2	0.44

Notes. The close similarity of the mean and the low standard deviation for colors, ages, and metallicities indicate their fair repeatability and reproducibility by the two photometric systems and the two age–metallicity estimation methods.

$$\mathrm{PC2} = 0.345[\mathrm{Fe/H}] - 0.935\tau + 0.047(uz - vz) - 0.061(bz - yz) + 0.020(vz - yz), \quad (5)$$

where τ is the age of the stellar population in Gyr. Metallicity terms in both equations have almost equal weights, but the weights for the age terms are smaller in the first equation compared to the second. The SSP models reflect the ages and metallicities of star clusters and the summation of the star clusters reflects the age and metallicity of the composite stellar populations such as ellipticals. However, the low-order difference between globulars and ellipticals signals that the SSP assumption is an adequate approximation for many needs and that the stellar population in ellipticals must be of a simple form like a Gaussian distribution to produce a correlation (R05a). Since the filter system is more sensitive to metallicity than to age, the uncertainty due to age is greater than for metallicity which is 0.5 Gyr and 0.2 dex, respectively, as quoted by R05a.

The other model considered here for comparison is the GALEV (successor of the S02 models; Kotulla et al. 2009), a galaxy evolutionary synthesis model that produces a large grid of galaxy SED templates in a chemically consistent manner. The GALEV offers only five metallicity models: −1.7 dex, −0.7 dex, −0.3 dex, 0.0 dex, and 0.3 dex. For more details, refer to Kotulla et al. (2009).

3.2. Comparison of Colors, Model Ages, and Metallicities

This section discusses the results for the following tests to check: (1) the repeatability of the observed narrowband colors using the two filter systems, the Strömgren and the modified Strömgren systems, to assess the quality of the observed colors and (2) the agreement of the estimated ages and metallicities using two different techniques: PCA and the GALEV models.

Unfortunately, from the available data, only six bright, isolated galaxies were found to be common in all three data sets. These galaxies are in the magnitude range of $14.1 \leqslant m_{5500} \leqslant 15.5$ ($-20.7 \leqslant M_{5500} \leqslant -19.3$). Figure 1 shows the combined bz (4675 Å) image of A779 observed with the Steward 90 Prime in 2004 April with the chosen galaxies numbered 1–6. Table 2 gives the comparison of colors and M_{5500} brightness between the three sets of observations along with their age and metallicity estimations using PCA and the GALEV models. The mean displayed for each set of galaxy colors, ages, and metallicities represents their close nature, and hence smaller uncertainties.

Table 3 presents the standard deviations (σ) in the measurements of the narrowband colors and their respectively derived ages and metallicities using the two evolutionary models. A low

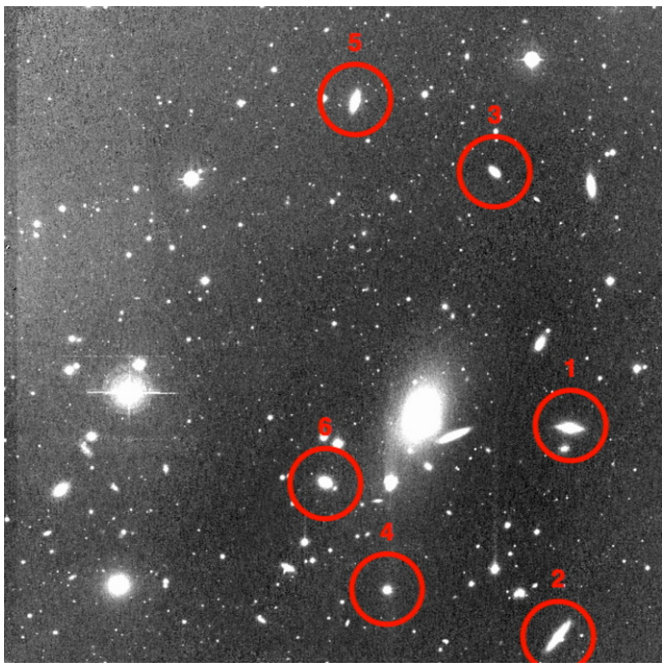

Figure 1. A779 cluster at $z = 0.023$ with a central cD galaxy (NGC 2832) stretched in the N–S direction. This 0.′3 × 0.′3 combined image of three bz (4675 Å) filter images was observed in 2004 at Steward Observatory, AZ. The figure shows the six common galaxies in all three data sets which are compared in Tables 2 and 3.

(A color version of this figure is available in the online journal.)

standard deviation conveys the quality of repeatability of the observed colors. The $(uz - vz)$ color has the largest standard deviation (σ) value of 0.09 among the three because of its sensitivity to the atmosphere, whereas the $(bz - yz)$ and $(vz - yz)$ colors have 0.02 and 0.03, which are small and expected due to photometric errors and the atmospheric extinction. The mean σ value for the ages and metallicities determined by the PCA method are found to be 0.36 Gyr and 0.04 dex, respectively, within the uncertainty limits (0.5 Gyr in age and 0.2 dex in metallicity) as quoted by R05a. On the other hand, GALEV estimates the same two parameters with an accuracy of 0.44 Gyr and 0.2 dex for the age and metallicity, respectively. The means of the standard deviation of the GALEV estimated ages and metallicities are found to be larger compared to those from PCA, which are due to GALEV's limited range of model metallicities (−1.7, −0.7, −0.4, 0.0, and 0.4 dex) and a significant effect of the age–metallicity degeneracy, which could be relieved with the use of a high-resolution spectral library and the application of

PCA. Nevertheless, the low values of σ indicate a fair similarity between the two model age and metallicity estimations.

The observed differences in colors, ages, and metallicities could be explained by the following:

1. The uncertainties in the colors (of the order of a few hundredths of a magnitude) could be due to the atmospheric extinction and photometric errors.
2. The uncertainties of 0.5 Gyr in age and 0.2 dex in metallicity can result from the interpolation between the limited range of the S02 models, and the iterative method used by the PCA technique.
3. The ability of the individual models, and the limited range of the model metallicities of S02 and GALEV to reproduce the correct ages and metallicities from the observed galaxy colors can also introduce errors.
4. The effect of the prevailing age–metallicity degeneracy can further affect the results, especially in the GALEV models as it is not supported by any additional technique to separate the age effects from those of metallicity.

The effect of the age–metallicity degeneracy has been a major obstacle in all the stellar population evolutionary techniques in their accurate determination. The continuum color method supported by the PCA technique does, in fact, separate the age effects from the metallicity effects, but only to a certain extent (as shown by the standard deviation in Table 3). From Table 1 in R05a, close similarities in the specific colors for different age and metallicity SSPs can be found, for example, the $(uz - vz)$, $(bz - yz)$, $(vz - yz)$ colors for the $Z = -0.7$ dex, age = 6.02 Gyr are 0.713, 0.232, 0.360 and for $Z = -0.4$ dex, age = 4.06 Gyr with 0.718, 0.231, 0.375, respectively, are quite similar. Likewise, the SSP with $Z = -0.4$ dex, age = 6.02 Gyr, $(uz - vz)$, $(bz - yz)$, $(vz - yz)$ colors are 0.731, 0.256, 0.443 which are similar to $Z = -0.7$, age = 8.12 Gyr (with colors 0.727, 0.258, 0.432) and $Z = -0.7$, age = 10.08 Gyr (0.731, 0.260, 0.442).

Observationally, these color differences are well within the photometric uncertainty limits, which may result in incorrect estimations of the ages and metallicities of the SSPs. When considering a galaxy with the luminosity-weighted mean age and metallicity, these uncertainties are masked under the galaxy's overall age and metallicity. Obviously, this would depend upon the mass of the SSP (of a certain age and metallicity) which is the major contributor to the galaxy's overall age and metallicity. For example, in an old red galaxy which is a mixture of several SSPs (mostly old), it is very difficult to estimate the uncertainty of the SSP with incorrect age and metallicity because of the indistinguishability of the masses of different SSPs which form a single galaxy age and metallicity (Rakos et al. 2008). However, for a young galaxy with most of its star clusters primarily young with perhaps similar ages and metallicities, the uncertainty in such a case would be comparatively higher; this error and its effect are more pronounced in studies of individual star clusters and young galaxies.

Nevertheless, our analysis of different SSP ages and metallicities conveys that the degeneracy is still prevailing. In order to minimize the effect of this degeneracy, it is important to reduce the photometric uncertainties by avoiding very faint and diffused (galaxies with large gas content) objects and choosing judicious apertures depending upon the brightness and the type of galaxy, as performed in our studies. Since our photometric studies are based on Strömgren (or modified Strömgren) filters that are well known for their age and metallicity sensitivity and are supported by the PCA technique, the effect of degeneracy observed here is not as severe as reported by spectroscopic and broadband observations. Therefore, the degeneracy is only relieved, not eliminated.

4. DISCUSSION

4.1. Spectrophotometric Classification

Using the PCA classification for galaxies, based on the narrowband colors, our sample segregates into four main categories: ellipticals (E, passive, red objects), S−types such as S0s (transition objects between ellipticals and spirals), spirals (S, objects with a star formation rate equivalent to the disk galaxies), and S+ (starburst systems). By comparing nearby galaxy observations with the SED models, the divisions along the PC1 axis are made such that the S galaxies are the systems with a spiral star formation rate of about 1 $M_{\odot}$ yr^{-1} and the S+ objects correspond to starburst rates of about 10 $M_{\odot}$ yr^{-1} (Rakos et al. 1996). Once again, one must remember that these star formation rates represent the mean over the last few gigayears, and not the current star formation rate, as reflected by the optical emissions of the dominant stellar population. The colors displayed by the red E systems show no evidence of star formation in the past 4–5 Gyr. The S− class of objects is the transition galaxies that show no sharp division between the E and S galaxies. These galaxies show slightly bluer colors (statistically) from the passive E galaxies; however, the difference could be due to a recent, low-level burst of star formation or later epoch of galaxy formation or an extended phase of early star formation or even lower mean metallicity (i.e., the color–magnitude effect). The PC2 is able to classify signatures of non-thermal continuum colors of the active galactic nuclei into A+, A, and A- types (for more descriptions see Steindling et al. 2001 and Rakos et al. 2007).

The PCA classification scheme shows that our A779 sample constitutes one-third (31%) ellipticals, 40% S− types (S0s) which form the majority, 24% S class galaxies, and just 4% S+ galaxies. This classification scheme, based on the PC equations using the narrowband color indices, agrees with the results of Hwang & Lee (2008), finding greater numbers of the early-type (ellipticals and S0s) galaxies than the late types. Table 4 lists the A779 member galaxies with their names, R.A., declination, and photometric errors. Since Rakos et al. (2008) have previously studied and analyzed the color–color and color–magnitude relations for the galaxies in A779, we refrain from repeating the same inference in this paper. For more detailed color–color and color–magnitude relations, see Rakos et al. (2008).

4.2. Spectrophotometric Class–Density Relation

Even though the continuum colors are integrated in the PC equations (needed for galaxy classification), a majority of the galaxies classified using this technique are found to match the morphological classifications well. The idea is to build a close one-to-one relationship between the spectrophotometric classification and the morphology (Rakos & Schombert 2005b). Figure 2 shows the variation in the density of spectrophotometric galaxy classes as a function of radial distance from the A779 cluster core. The galaxy density as a function of spectrophotometric class is binned in an area of 0.1 Mpc^2 extending out from the cluster center, resembling the density–morphology relation (Dressler 1984; Smith et al. 1997). Due to the small sample of S+ objects (and the similarities in their star formation rates), we have combined them with the S class of objects. The figure also displays large errors for different spectrophotometric class due

Table 4
A779 Galaxy Names, R.A., decl., and Photometric Errors for $(uz - vz)$, $(vz - yz)$, and $(bz - yz)$

No.	Galaxy Names	R.A.	Decl.	$\pm(uz - vz)$ (mag)	$\pm(vz - yz)$ (mag)	$\pm(bz - yz)$ (mag)
1	NGC 2827	09:19:19	33:52:51	0.003	0.004	0.003
2	SDSS J091920.23+335110.6	09:19:20	33:51:11	0.053	0.037	0.221
3	NGC 2825	09:19:22	33:44:34	0.001	0.002	0.002
4	NGC 2826	09:19:24	33:37:26	0.001	0.002	0.002
5	SDSS J091927.47+334808.4	09:19:27	33:48:07	0.115	0.110	0.060
6	SDSS J091929.94+335825.9	09:19:29	33:58:25	0.030	0.026	0.022
7	NGC 2829	09:19:30	33:38:54	0.062	0.006	0.005
8	SDSS J091930.47+334323	09:19:30	33:43:23	0.152	0.141	0.079
9	SDSS J091932.98+335553.4	09:19:32	33:55:52	0.122	0.109	0.075
10	NGC 2828	09:19:34	33:53:17	0.003	0.003	0.002
11	SDSS J091935.79+334346.6	09:19:35	33:43:46	0.021	0.019	0.020
12	SDSS J091938.35+334823.8	09:19:38	33:48:24	0.065	0.038	0.041
13	SDSS J091939.31+334612.1	09:19:39	33:46:11	0.069	0.042	0.044
14	2MASX J09193944+3357130	09:19:39	33:57:12	0.008	0.006	0.006
15	NGC 2830	09:19:41	33:44:17	0.001	0.002	0.002
16	SDSS J091941.69+334820	09:19:41	33:48:21	0.022	0.019	0.022
17	SDSS J091942.21+334137.8	09:19:42	33:41:38	0.019	0.014	0.015
18	SDSS J091942.98 + 334839.5	09:19:42	33:48:39	0.102	0.006	0.006
19	SDSS J091943.54+333656.5	09:19:43	33:36:57	0.028	0.026	0.019
20	NGC 2831	09:19:45	33:44:42	0.001	0.001	0.001
21	SDSS J09194559+3343124	09:19:45	33:43:12	0.006	0.006	0.005
22	NGC 2832	09:19:46	33:44:59	0.001	0.001	0.001
23	2MASX J0919478+334604	09:19:47	33:46:05	0.011	0.009	0.009
24	1200-06282293	09:19:48	33:43:44	0.051	0.024	0.019
25	2MASX J09195225+3338584	09:19:52	33:38:59	0.003	0.003	0.002
26	1200-06282758	09:19:55	33:40:51	0.033	0.023	0.016
27	SDSS J091957.23+334047.5	09:19:57	33:40:47	0.141	0.016	0.014
28	NGC 2833	09:19:57	33:55:39	0.001	0.001	0.001
29	SDSS J092000.91+334225.3	09:20:00	33:42:25	0.024	0.021	0.021
30	SDSS J092002.6+335804.8	09:20:02	33:58:05	0.014	0.015	0.014
31	NGC 2834	09:20:02	33:42:37	0.002	0.002	0.002
32	SDSS J92004.04+334748.3	09:20:04	33:47:48	0.111	0.100	0.065
33	SDSS J092005.14+334516.4	09:20:05	33:45:15	0.113	0.098	0.076
34	2MASX J09200859+3339424	09:20:08	33:39:42	0.003	0.003	0.002
35	SDSS J92025.35+335151.6	09:20:25	33:51:52	0.101	0.077	0.076
36	SDSS J92027.84+335035.2	09:20:27	33:50:35	0.020	0.020	0.013
37	2MASX J0920286+333902	09:20:28	33:39:00	0.007	0.009	0.009
38	SDSS J92030.17+333925.4	09:20:30	33:39:25	0.093	0.088	0.057
39	NGC 2839	09:20:36	33:39:03	0.001	0.002	0.002
40	SDSS J92037.04+334222.0	09:20:37	33:42:21	0.011	0.010	0.009
41	SDSS J092041.84+334339.9	09:20:41	33:43:40	0.069	0.022	0.016
42	2MASX J09204457+3346220	09:20:44	33:46:22	0.004	0.005	0.004
43	MCG +06-21-024	09:20:45	33:42:16	0.004	0.004	0.003
44	SDSS J092047.1+333953.4	09:20:47	33:39:53	0.035	0.032	0.024
45	SDSS J092048.04+334046.8	09:20:48	33:40:47	0.007	0.006	0.005

to the fewer A779 galaxies that are spread sparsely across the cluster distance.

The figure shows the innermost regions of A779 which are dominated by the red population, largely by the S− and some E types, in agreement with Wilson & Vallée (1982) and Fanti (1984). The star-forming blue populations, the S/S+ types, avoid cluster cores and are found to populate at 0.2 Mpc from the center, and their density declines with increasing distance. Most of the passive galaxies are known to occupy regions very close the cluster core, but, surprisingly, the E and the S− types also show their presence at distances of 0.3 Mpc from the center. These galaxies could represent the second generation of young red population with a small mass of star-forming populations.

Another inference that can be gathered from Figure 2 is with respect to the changing ratio of the blue to red cluster galaxies, the so-called Butcher–Oemler effect (Butcher & Oemler 1984). Blue galaxies, those concentrated at 0.2 Mpc from the cluster center are slowly turning into red, like spirals becoming Sa types (represented by the S− types occupying the region near 0.3 Mpc from the cluster center). These S− galaxies have low star formation rates, and as they age, their star formation ceases and they drift to the clustercentric regions, joining the S0 populations at 0.1 Mpc. The E class of red galaxies cannot be the rightful candidates for the blue cluster galaxies because the majority of their mass consists of old (12 Gyr) populations.

4.3. Ages and Metallicities of A779 Cluster Galaxies

The optical colors of galaxies reflect information that pertains to the photospheres of the stars present in stellar populations, and any change in these colors would indicate a change in these stellar populations. Since stellar populations keep a record

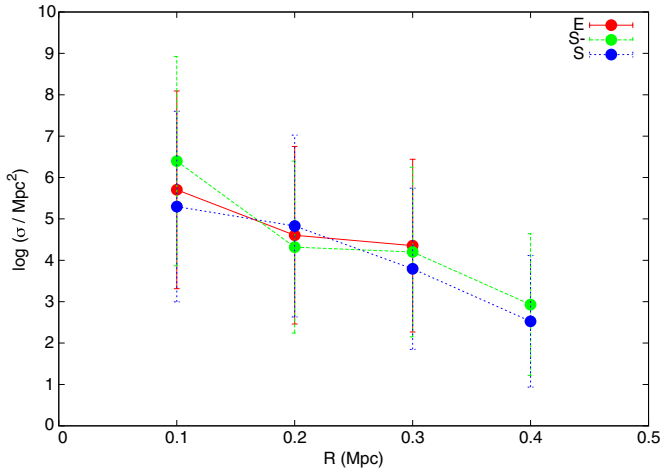

Figure 2. Projected radial galaxy density for each galaxy spectrophotometric class as a function of radial distance from the cluster center. The number of spectrophotometric galaxy types are binned in an area of 0.1 Mpc^2 from the cluster center. The plot displays the central cluster regions which are occupied by the old S galaxies that fall almost sharply with a slight increase in the blue S/S+ star-forming galaxies at about 0.2 Mpc from the center. At 0.3 Mpc, there is a slight increase in the second generation of the young S and some E galaxies.

(A color version of this figure is available in the online journal.)

of most of their evolution, by studying the H-R diagram (or color–magnitude diagrams) of these stars, it is possible to constrain the star formation history (age) and enrichment (metallicity) from their initial formation (Grebel 2005). After testing for the precision of the estimated ages and metallicities using PCA and the GALEV models, we present here the luminosity-weighted SSP mean ages and metallicities for A779 member galaxies using the PCA method. These ages and metallicities are shown in Figure 3 along with their correlation with M_{5500} luminosity (mass). The typical uncertainties for the ages, metallicities, and M_{5500} are 0.5 Gyr, 0.2 dex (R05a), and 0.15 mag, respectively, displayed at the corner of each plot. The differing sizes of the data points in the plots show the true dispersions in the averages of the SSP ages and metallicities, and are not uncertainties. Since these true dispersions depict the standard deviation of the averaged SSP ages and metallicities, they would represent the star formation histories in such a way that the higher the dispersion due to longer star formation history, the bigger the size of the data point would be.

Directly visible from the plot in Figure 3 is the "bimodality" of two clumps of populations divided by their age, metallicity, and mass. The first group of objects is the older mixture of the early-type ellipticals and the S0s, with a mean age of 9 Gyr, classified as the classic red-sequence galaxies. These red-sequence galaxies show a horizontal spread in metallicity ranging from −0.5 dex to slightly above solar. The second group is the blue-sequence galaxies, which show a mixture of the S− class, spirals (S), and the starburst (S+) objects, which are younger (5–8 Gyr) than the red-sequence galaxies. Also, compared to the older galaxies, these younger galaxies show relatively stronger chemical evolution with Z ranging from −2.1 dex to slightly above −0.5 dex.

Interestingly, the galaxy quantities, like the age, M_{5500} (mass), and metallicity, are found to correlate well with one another; the low-mass galaxies are metal-poor ($Z \leqslant -0.5$ dex), whereas the metal-rich ($\sim Z_{\odot}$) galaxies are more massive and older galaxies. Galaxies with ages of 8 Gyr are brighter than $M_{5500} = -18$ mag

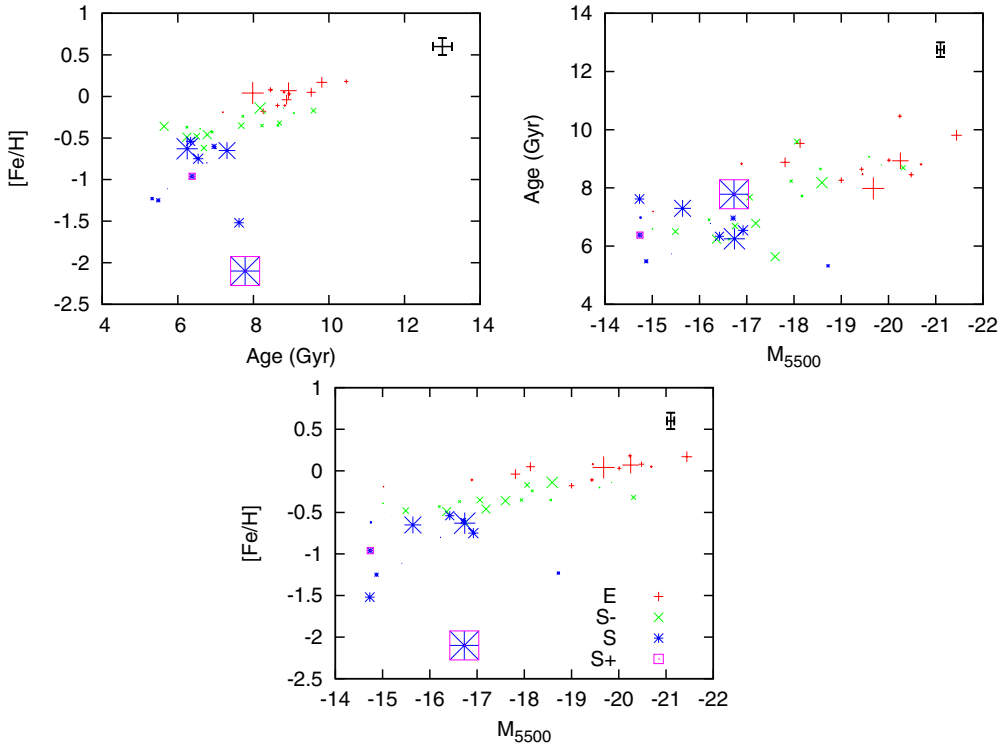

Figure 3. Age, Z, mass (luminosity) plot for A779 galaxy members. Each plot compares the SSP luminosity-weighted mean, age, and metallicities for all 45 A779 member galaxies. Different galaxy classes are displayed with different colors (E types in red pluses, S− in green crosses, S in blue asterisks, and S+ in purple squares). The typical uncertainties are 0.5 Gyr for age, 0.15 mag for M_{5500} and 0.2 dex for Z, which are shown at the corner of each individual plot. The varying size of individual data points gives true dispersion in the averages. Two distinct groups of populations are observed, one with a mean age of 9 Gyr, represented by the old, massive, metal-rich, red populations, and the other with a mean age of 6.7 Gyr, which is the young, low-mass, metal-poor set of blue populations.

(A color version of this figure is available in the online journal.)

with near-solar metallicities, whereas the young, low-mass galaxies are metal-poor with $Z < -0.5$ dex. This phenomenon of decreasing mass with age is referred to as the "downsizing" scenario of galaxy formation (Bundy et al. 2005; Mateus et al. 2006). The best demonstration of the downsizing effect is the color–magnitude relation diagram from $z = 0.7$ clusters by De Lucia et al. (2004), which shows the deficiency of low-luminosity red galaxies between $M_v = -19$ mag and -17 mag. Studies from Rakos et al. (2007) show that only 5%–10% of the galaxy's mass needs to be involved in star formation to produce the spiral-like colors, as seen in De Lucia et al.'s diagrams. Given that $z = 0.7$ corresponds to 6 Gyr ago, this would produce the current generation of low-luminosity cluster ellipticals with 10% of their galaxy mass in a 6 Gyr population plus the remaining 90% of their galaxy mass in a 12 Gyr population (Rakos et al. 2007). Convolving these values in our SED models reveals that the luminosity-weighted mean age of such a galaxy would be about 10 Gyr, as observed in the plots of Figure 3. The blue population (S−, S, and S+ class) consists of the star-forming galaxies which slowly fade to the low-mass S− class of the S0s with traces of star formation. The blue colors of this galaxy type show ongoing star formation with a majority of their stellar mass in the old stellar populations and a substrate of the young (less than 1 Gyr) stellar population that combine to produce an integrated age of 5–7 Gyr. Once again, using the SED models we find that about 10% of the mass of these blue galaxies can be in a 1 Gyr stellar population and the rest in a 12 Gyr one to produce the observed colors of about 6 Gyr.

Thomas et al. (2002) claim that [α/Fe] ratios are highest in the oldest galaxies of his sample, which would imply a short initial duration of star formation for the old galaxies. This also conveys that the initial star formation duration increases with decreasing mass, as evident from our results which show, on average, the large sizes of the data points for the young, blue-sequence galaxies compared to the old population. A set of blue asterisk symbols in Figure 3 represents the S (spiral) population; these are low-mass, young galaxies with metallicities between -0.5 dex $\leqslant Z \leqslant -1$ dex and an age range of 5 Gyr $\leqslant \tau \leqslant 8$ Gyr. A careful inspection of these S galaxies with their extended star formation histories and their location from the cluster confirms the 21 cm radio study of Solanes et al. (2001), that the inner and outer 1 Abell radius ($\sim$1 Mpc) of this cluster has spirals with significantly low H I content. This could be due to the star formation events that transformed the H I gas to H_2 to form stars in these low-mass spirals localized at 0.3 Mpc from the cluster center.

The presence of only two starburst galaxies in our sample, one very close to the cluster core and the other at the outer regions of the cluster, is somewhat strange. As starbursts represent a collection of young objects (OB associations of a few million years old), their analysis is not quite reliable, as our technique is only effective for stellar populations with ages >3 Gyr. The luminosity-weighted mean ages of the two starbursts in our sample are found to be 6.4 Gyr and 7.8 Gyr, at 0.06 Mpc and 0.3 Mpc from the cluster center, respectively. The presence of a starburst galaxy near the cluster core could be ruled out as a projectional effect, since it is highly unlikely for a starburst system to be actively forming stars at such close proximity to the cluster core. However, the other at 0.3 Mpc from our morphological analysis performed on our images shows similarities to an irregular disk system with high star formation history. While dealing with systems that have high star formation rates and their bluer colors, it is possible that our spectrophotometric classification scheme miscategorizes some high star-forming spirals/irregular disk systems as starbursts because of the close resemblance between the galaxies in the S and the S+ categories.

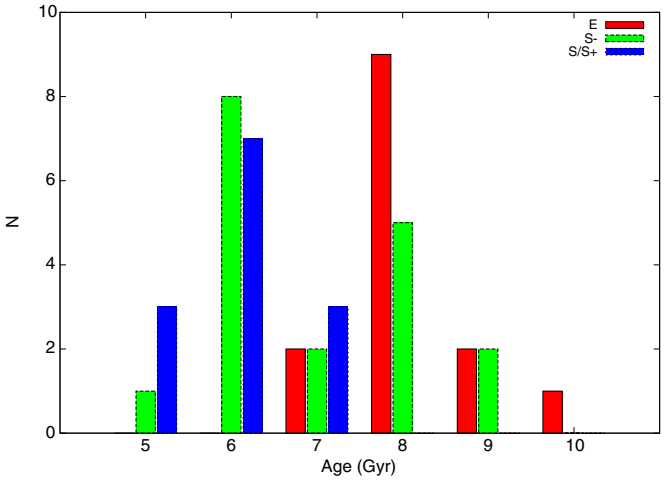

Figure 4. Histogram of galaxies of different ages as a function of spectrophotometric galaxy types: E (red), S−(green), S (blue). The S and the S+ objects are combined and represented as S type. A clear bimodality of old and young galaxy populations are observed at 6 and 8 Gyr.

(A color version of this figure is available in the online journal.)

4.4. Spectrophotometric Class–Age Histogram

Figure 4 shows a normalized histogram of age for different spectrophotometric classes (in steps of 1 Gyr above 5 Gyr) of A779 galaxies. In agreement with the above discussion, this figure, in general (ignoring the galaxy classification), presents the bimodality of the old population that peaks at 8 Gyr and the young population at 6 Gyr. Also visible in this histogram, within the two groups there are differences in age for different spectrophotometric types, but when observed as a function of spectrophotometric types, the bimodality feature is observed only for the S− types (S0s), as the S0s form the majority in our cluster sample. The two groups of S0s show peaks for young 6 Gyr (about 8 in number) galaxies, which match the peak of the maximum number of the star-forming S/S+ types, and for the 8 Gyr old S0 galaxies, which match with the maximum of the E galaxies. This clearly shows that the S0s are the transitional galaxy types that bridge the gap between the red- and blue-sequence galaxies. The old (8 Gyr) E galaxies are mostly non-star-forming bulge systems, whereas the second group of young galaxies consists of the S−, S, and S+ galaxies that show a mixture of old, bulge system plus a younger disk population.

With regard to the star formation history, the second group of the S− galaxies does show the possibility that a small percentage of their mass are star-forming, which produces their younger mean ages. The determination of the exact nature of these young S− classes is difficult because our technique is unable to distinguish, using SED models, between star formation history scenarios where the young population is composed of a young age due to (1) later formation redshift, (2) longer initial star formation duration, or (3) a later burst of star formation (a frosting event; Trager et al. 2000).

4.5. Age/Metallicity–Distance Relation

Figure 5 presents the variation in the age and metallicity of the cluster galaxies as a function of clustercentric distance for different spectrophotometric classes and their star formation

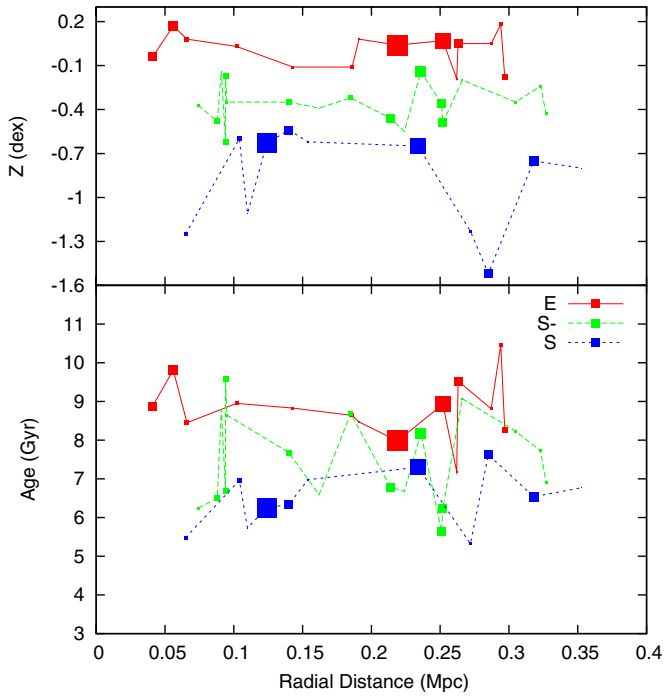

Figure 5. Radial change in galaxy age and metallicity as a function of spectrophotometric class and star formation history. The random distribution of galaxies shows no trend in separation by age and metallicity from the cluster center reflecting poor dynamical evolution of the A779 cluster.

(A color version of this figure is available in the online journal.)

history. Due to lack of sufficient sky coverage, we are restricted to analyzing galaxies within 0.4 Mpc of the cluster center. Unlike in the evolved clusters (e.g., A1185, Coma, A2218), the plot shows that A779 shows no significant trend between the galaxy age with distance from the cluster center and the old early types are distributed randomly across the cluster. The E galaxies near the cluster core are about 9 Gyr, which vary only slightly to 8 Gyr in age up to a distance of 0.25 Mpc, and then rise to 10 Gyr at 0.3 Mpc. A similar trend is also observed for the S− types with a 2 Gyr dip in age for galaxies near the core to a distance of 0.25 Mpc and again a 2 Gyr rise for the galaxies at a distance of 0.35 Mpc. For the late types, the variation in age with distance is again very small, from 6 Gyr at 0.1 Mpc to about 7 Gyr at 0.4 Mpc.

As the galaxy age and metallicity behave in the same manner as observed in Section 4.3, it is not surprising to expect the trend of metallicity–distance to be very similar to the age–distance relation, but compared to the haphazard pattern of the age–distance plot, the metallicity shows slightly organized separation for the different spectrophotometric classes with distance such that the E galaxies have near-solar metallicities, the S− types have metallicities of about −0.4 dex, and the S/S+ objects have metallicities of −0.8 dex. Since different galaxy types evolve differently under the influence of differing environmental effects across the cluster radial distance, we analyzed for the differential variation in metallicity for 1 Gyr change in age for the three spectrophotometric classes across the radial distance. We note a significant change in metallicity for the E types at 0.1–0.2 Mpc; the maximum variation in metallicity for the S− class is observed at 0.2–0.3 Mpc and 0.25–0.4 Mpc for the S/S+. Interestingly, the region of 0.2–0.4 Mpc from the cluster core is the most dense with most (22) of our galaxy samples, which, on average, show large star formation histories. Clearly, considering the direction toward the increasing differential variation in metallicity and the presence of a large number of galaxies with high star formation histories, the region beyond 0.25 Mpc seems to be the breeding ground with a lot of active physical processes to enhance the star formation in the young low-mass galaxies (S types with ages between 5–7 Gyr and the second generation of the S− types of 5–9 Gyr), as also confirmed by our Figure 2. As a further confirmation, these low-mass, young star-forming galaxies present a scattered population in Figure 3, which distinctly shows the physical processes active in the galaxies located in these regions. The presence of two large E data points in this region was morphologically analyzed to find their resemblance to the E5–E7 elliptical galaxy types that are known to be misclassified S0s (van den Bergh 2009).

As an overall analysis of A779 using the modified Strömgren photometry, we find that the cluster is fairly young, low-mass, and has a poor dynamical evolution which is reflected by its fewer members, disorganized distribution of galaxies by age and metallicity across the radial cluster distance, and the low star formation histories of the member galaxies compared to other dynamically evolved clusters.

5. CONCLUSION

In the first part of this paper, we tested six galaxies in A779 for the repeatability of colors using the three sets of observations with the two filter systems: Strömgren and modified Strömgren. Our test shows a fair repeatability that reproduces similar ages and metallicities within an uncertainty of 0.5 Gyr in age and 0.2 dex in metallicity, as presented in Tables 2 and 3. The ages and metallicities are estimated using the PCA method and the GALEV models. The mean standard deviation σ for colors $(uz - vz) = 0.09$, $(bz - yz) = 0.02$, and $(vz - yz) = 0.03$ are found. The σ for the measured ages and metallicities from the PCA method are found to be 0.04 Gyr and 0.36 dex, respectively, and from GALEV 0.2 Gyr and 0.44 dex, respectively.

The small observed color differences could be accounted due to (1) the photometric errors, (2) the slight variation in the two filter transmission curves, and (3) the λ-dependent flux measurement of the modified Strömgren system. The uncertainties in the estimated ages and metallicities could be due to (1) the quality of the solutions obtained by the PCA iterative method, (2) the ability to accurately estimate ages and metallicities by the S02 and the GALEV models, (3) their limited model metallicity range to reproduce proper ages and metallicities, (4) the effect of the age–metallicity degeneracy problem in the GALEV models, and (5) the errors due to interpolation for the S02 models using the PCA method.

Careful inspection of the SSP colors for different ages and metallicities, enlisted in Table 1 of R05a, shows close similarities between one another within the limits of photometric uncertainties. This conveys that even with the application of PCA, to separate the age effects from the metallicity effects, the degeneracy still persists, but the effect is not as significant as observed from the spectroscopic and broadband observational studies. Therefore, the age–metallicity degeneracy using the narrowband continuum color method is only relieved, not completely eliminated.

In our second part, we analyze the X-ray and radio-quiet, poor A779 cluster with 45 member galaxies detected by our photometric method in the 1° field of view. We note a clear correlation of galaxy age, metallicity, and luminosity (mass) to understand their formation scenarios with effect to the cluster environment. Using our spectrophotometric classification method, we find that the high-mass, luminous (E/S−) galaxies

have a luminosity-weighted mean age of 9 Gyr (± 0.5 Gyr) and the low-mass, fainter (S/S+ and the young E/S−) galaxies have a mean age of 6.7 Gyr (± 0.5 Gyr). The older, red-sequence galaxies show higher mean metallicities of −0.18 dex (± 0.2 dex), whereas their younger, blue-sequence counterparts are slightly metal-poor with a mean of −0.63 dex (± 0.2 dex). The galaxies with the higher mean age and metallicity are more massive than the younger, low mean metallicity objects. The older galaxies comprise mostly ellipticals (E class) and the S0s (S− class), whereas the young galaxies are a mixture of the spirals, disks/irregulars (S class), the starburst systems (S+), and the low-mass red sequence of galaxies.

We observe the usual trend of galaxy age with mass such that the older, red population has a single short epoch of star formation and this initial duration of star formation increases with decreasing mass, a weaker version of the downsizing effect (Gallazzi et al. 2006). A similar phenomenon is also observed by the smaller spread in metallicity for the red-sequence galaxies, hinting at the common formation epoch for these populations, and the higher luminosities point to their massive nature. The scatter in the second group (blue sequence) of galaxies points to the ongoing physical processes that show an extended chemical evolution with a longer epoch of star formation. The star formation histories of the second group of galaxies also show the presence of a few low-mass S− galaxies which have a small percentage (5%–10%) of young, low-mass star-forming population galaxies inside the old S0 galaxies.

The cluster's innermost regions are occupied by the old, red-sequence galaxies, whereas the blue star-forming galaxies are present at 0.2 Mpc from the cluster core. These low-mass S/S+ galaxies represent the Butcher–Oemler galaxies that would fade to the red Sa types to join the other second generation of the S− types at 0.3 Mpc from the cluster center. As the traces of star formation cease with age, these S− galaxies would drift to settle with the other S0s observed close to the cluster center at 0.1 Mpc.

The correlation between the age (and metallicity) with radial distance from the center, as a function of spectrophotometric class and star formation history, is poor. The old early-type galaxies follow a random distribution by age and metallicity across the cluster distance from the center. However, the late-type, young galaxies do show a slight trend of 6 Gyr galaxies at 0.1 Mpc to about 7 Gyr at 0.4 Mpc. The metallicity–distance trend is similar to that of the age–distance relation. The plot confirms our idea about the blue galaxies which are actively forming stars at 0.25 Mpc, slowly drifting to the cluster edges as they age and eventually fall into the S− types at the cluster center. The region beyond the 0.25 Mpc appears to be the breeding ground for low-mass galaxies with a lot of active physical processes leading to a larger chemical evolution and enhanced star formation.

Our overall assessment, which is in agreement with other studies using different wavelengths and methods, indicates that cluster A779 is a young, low-mass, dynamically poor cluster with a passive cD galaxy (NGC 2832) close to the cluster center. Our technique of modified Strömgren photometry has also shown an in-depth analysis of the cluster galaxies with age and metallicity measurements and their correlation with spectrophotometric galaxy types, density, star formation history, and the cluster's radial distance. This analysis proves the technique's ability to study galaxy clusters at low- and intermediate-z.

We are grateful to our colleague and mentor, Karl Rakos (86), who passed away on 2011 October 31, and we dedicate this paper to him and his contributions to the field. We thank the team at Steward Observatory, University of Arizona for the time allocation and the assistance and support that they provided. This work is supported and funded by the University of Vienna within the Initiative College "Cosmic Matter Circuit" (IK 538001).

REFERENCES

Bundy, K., Ellis, R. S., & Conselice, C. J. 2005, ApJ, 625, 621
Butcher, H., & Oemler, A. 1984, ApJ, 285, 426
David, L. P., Slyz, A., Jones, C., et al. 1993, ApJ, 412, 479
De Lucia, G., Kauffmann, G., & White, S. D. M. 2004, MNRAS, 349, 1101
Dressler, A. 1984, ARA&A, 22, 185
Duc, P.-A., Braine, J., Lisenfeld, U., Amram, P., & Brinks, E. 2002, Ap&SS, 281, 347
Fanti, R. 1984, in Clusters and Groups of Galaxies, ed. F. Mardirossian, G. Giuricin, & M. Mezzetti (Boston, MA: Reidel), 185
Ferreras, I., Charlot, S., & Silk, J. 1999, ApJ, 521, 81
Fischer, D., Franx, M., & Illingworth, G. 1996, ApJ, 459, 110
Gallazzi, A., Charlot, S., Brinchmann, J., & White, S. D. M. 2006, MNRAS, 370, 1106
González, J. J. 1993, PhD thesis, Univ. California, Santa Cruz
Grebel, E. K. 2005, in IAU Collog. 198, Near-field Cosmology with Dwarf Elliptical Galaxies, ed. H. Jerjen & B. Binggeli (Cambridge: Cambridge Univ. Press), 1
Gunn, J. E., & Gott, J. R. 1972, ApJ, 176, 1
Hamuy, M., Suntzeff, N., Heathcote, A., et al. 1994, PASP, 106, 566
Huchra, J. P., Geller, M. J., Clemens, C. M., Tokarz, S. P., & Michael, A. 1992, Bull. Inf. Cent. Donnees Stellaires, 41, 31
Hwang, H. S., & Lee, M. G. 2008, ApJ, 676, 218
Jones, C., & Forman, W. 1984, ApJ, 276, 38
Kellogg, E., Murray, S., Giacconi, R., Tananbaum, H., & Gursky, H. 1973, ApJ, 185, 13
Kennicutt, R. C. 1992a, ApJS, 79, 255
Kennicutt, R. C. 1992b, ApJ, 388, 310
Kinney, A., Calzetti, D., Bohlin, R., et al. 1996, ApJ, 467, 38
Koleva, M., Prugniel, Ph., Ocvirk, P., Le Borgne, D., & Soubiran, C. 2008, MNRAS, 385, 1998
Kotulla, R., Fritze, U., Weilbacher, P., & Anders, P. 2009, MNRAS, 396, 462
Massey, P., & Gronwall, C. 1990, ApJ, 358, 344
Mateus, A., Sodré, L., Cid Fernandes, R., et al. 2006, MNRAS, 370, 721
Oegerle, W. R., & Hill, J. M. 2001, AJ, 122, 2858
Rakos, K. D., Maindl, T., & Schombert, J. 1996, ApJ, 466, 122
Rakos, K. D., Norbert, F., & Schombert, J. M. 1988, ApJ, 328, 463
Rakos, K. D., & Schombert, J. M. 2005a, PASP, 117, 245
Rakos, K. D., & Schombert, J. M. 2005b, AJ, 130, 1002
Rakos, K., Schombert, J., Maitzen, H. M., Prugovecki, S., & Odell, A. 2001, AJ, 121, 1974
Rakos, K. D., Schombert, J. M., & Odell, A. 2007, ApJ, 658, 929
Rakos, K. D., Schombert, J. M., & Kreidl, T. J. 1991, ApJ, 377, 382
Rakos, K. D., Schombert, J. M., & Odell, A. 2008, ApJ, 677, 1032
Sanchez-Blazquez, P., Gorgas, J., Cardiel, N., & Gonzalez, J. J. 2006, A&A, 457, 809
Schulz, J., Fritze, U., Möller, C. S., & Fricke, K. J. 2002, A&A, 392, 1
Smith, R. J., Lucey, J. R., Steel, J., & Hudson, M. J. 1997, MNRAS, 291, 461
Solanes, J. M., Manrique, A., García-Gomez, C., et al. 2001, ApJ, 548, 97
Steindling, S., Brosch, N., & Rakos, K. 2001, ApJS, 132, 19
Strömgren, B. 1966, ARA&A, 4, 433
Thomas, D., Maraston, C., & Bender, R. 2002, Ap&SS, 281, 371
Tinsley, B. 1980, Fund. Cosmic. Phys., 5, 287
Trager, S. C., Faber, S. M., Worthey, G., & González, J. J. 2000, AJ, 120, 165
van den Bergh, S. 2009, ApJ, 694, 120
Weilbacher, P., Duc, P.-A., Fritze-v Alvensleben, U., & Fricke, K. J. 2000, A&A, 358, 819
White, D. A., Jones, C., & Forman, W. 1997, MNRAS, 292, 419
Wilson, A. S., & Vallée, J. P. 1982, A&AS, 47, 601
Worthey, G. 1994, ApJS, 95, 107
Worthey, G. 1999, in ASP Conf. Ser. 192, Spectrophotometric Dating of Stars and Galaxies, ed. I. Hubeny, S. Heap, & R. Cornett (San Francisco, CA: ASP), 283
Zabludoff, A. I., Geller, M. J., Huchra, J. P., & Vogeley, M. S. 1993, AJ, 106, 1273